Journal of Engineering Mathematics **32:** 195–215, 1997.

Large-eddy simulations of shear flows

M. LESIEUR, P. COMTE, E. LAMBALLAIS, O. MÉTAIS and G. SILVESTRINI
LEGI/IMG, BP53, 38041 Grenoble-Cedex 09, France. e-mail: Marcel.Lesieur@hmg.inpg.fr

Received 5 November 1996; accepted in revised form 19 February 1997

Abstract. The general framework of large-eddy simulations (LES) is presented first, with Smagorinsky's model. Afterwards Kraichnan's spectral eddy-viscosity is introduced and it is shown how it can be handled for LES purposes in isotropic turbulence. The spectral eddy viscosity is generalized to a spectral eddy diffusivity. The nonlocal interaction theory is used to discuss the backscatter issue, and a generalization of spectral eddy coefficients is presented. This so-called spectral-dynamic model allows the representation of non-developed turbulence in the subgrid scales. Utilization of these spectral models in physical space is envisaged in terms of, respectively, the structure function and hyperviscosity models. Two applications of these models to shear flows are considered, namely the plane mixing layer and channel flow, with statistical results and information on the topology of coherent vortices and structures presented.

Key words: large-eddy simulation, turbulence, mixing layer, channel flow.

1. The need for large-eddy simulations

A direct-numerical simulation (DNS) of a turbulent flow has to take into account explicitly all scales of motion, from the largest, imposed by the existence of boundaries or the periodicities, to the smallest. The latter may be for instance the Kolmogorov dissipative scale $(\varepsilon/\nu^3)^{1/4}$ in three-dimensional isotropic turbulence, or the viscous thickness ν/v_* in a turbulent boundary layer.

It is well-known (see *e.g.* [1]) that the total number of degrees of freedom necessary to represent a turbulent flow through this whole span of scales is of the order of $R_l^{9/4}$ in three dimensions for isotropic turbulence, where R_l is the turbulent Reynolds number based on the integral scale. Right now, calculations done within reasonable computing times on the biggest machines take about 256^3 grid points. The improvement is very slow, and the Reynolds numbers thus attained with the aid of DNS are still several orders of magnitude lower than the huge Reynolds numbers encountered in natural situations.

The conclusion we draw is that, for a weakly viscous fluid, it is not possible in the near future (and perhaps not in the distant future either) to simulate explicitly all the scales of motion from the smallest to the largest. Generally, scientists or engineers are more interested in the description of the large scales of the flow, which often contain the desired information about turbulent transfers of momentum or heat. It is these large scales which will be simulated on the computer. This is done with LES (large-eddy simulation) techniques.

The paper is organized as follows. Section 2 presents the general framework of LES carried out in physical space, and the widely used model proposed by Smagorinsky [2]. Section 3 describes the concept of spectral eddy viscosity proposed by Kraichnan [3], and shows how it may be used for LES purposes. A generalization to a spectral eddy diffusivity for a scalar convected by the flow is discussed. This section presents results of the spectral eddy-viscosity model applied to decaying isotropic turbulence, with emphasis put upon infrared

backscatter. It introduces also a new model, the spectral-dynamic model, where the spectral eddy coefficients take into account non-developed turbulence in the subgrid scales. Section 4 shows how the spectral-space LES point of view may be recovered in physical space, in terms of the structure-function model and hyperviscosity models, respectively. Section 5 will mainly present applications of the filtered structure-function model to a temporal or spatially-developing plane mixing layer, and Section 6 will concern the plane turbulent channel studied with the spectral-dynamic model. In the two cases, statistical results as well as information regarding the topology of coherent vortices and structures will be given.

2. LES in physical space: the formalism

2.1. GENERALITIES

We present here the formalism for incompressible turbulence, with some indications of the way compressibility may be handled. We consider the philosophy of LES when the computation is carried out in physical space, using finite-difference or finite-volume methods. We assume first for the sake of simplification that the spatial discretization is cubic, Δx being the grid mesh. To the fields defined in the continuous space $\mathbf{x}$, we will associate filtered fields obtained through convolution with a filter $\bar{G}_{\Delta x}$, chosen so as to eliminate fluctuations in the motions of wavelength smaller than Δx. The filtered velocity and temperature are

$$\underline{\bar{u}}(\mathbf{x},t) = \int \mathbf{u}(\mathbf{y},t)\bar{G}_{\Delta x}(\mathbf{x}-\mathbf{y})\,\mathrm{d}\mathbf{y}, \tag{1}$$

$$\bar{T}(\mathbf{x},t) = \int T(\mathbf{y},t)\bar{G}_{\Delta x}(\mathbf{x}-\mathbf{y})\,\mathrm{d}\mathbf{y} \tag{2}$$

and the same for any quantity f (scalar or vectorial)

$$\bar{f}(\mathbf{x},t) = \int f(\mathbf{y},t)\bar{G}_{\Delta x}(\mathbf{x}-\mathbf{y})\,\mathrm{d}\mathbf{y} = \int f(\mathbf{x}-\mathbf{y},t)\bar{G}_{\Delta x}(\mathbf{y})\,\mathrm{d}\mathbf{y}. \tag{3}$$

We can easily check that such a filter commutes with temporal and spatial derivatives, so that the continuity equation for the filtered field holds. This is, however, no longer valid on irregular grids, where the filter has a variable width. Let $\mathbf{u}'$ and T' be the fluctuations of the actual fields with respect to the filtered fields

$$\mathbf{u} = \underline{\bar{u}} + \mathbf{u}'; \qquad T = \bar{T} + T' \tag{4}$$

and more generally $f = \bar{f} + f'$. A prime denotes field fluctuations at scales smaller than Δx (the 'grid scale'), and will thus be referred to as subgrid-scale fields.

Let us write the Navier–Stokes equations as

$$\frac{\partial u_i}{\partial t} + \frac{\partial}{\partial x_j}(u_i u_j) = -\frac{1}{\rho_0}\frac{\partial p}{\partial x_i} + \frac{\partial}{\partial x_j}\left\{\nu\left(\frac{\partial u_i}{\partial x_j} + \frac{\partial u_j}{\partial x_i}\right)\right\}. \tag{5}$$

After applying the filter, we get

$$\frac{\partial \bar{u}_i}{\partial t} + \frac{\partial}{\partial x_j}(\bar{u}_i \bar{u}_j) = -\frac{1}{\rho_0}\frac{\partial \bar{p}}{\partial x_i} + \frac{\partial}{\partial x_j}\left\{\nu\left(\frac{\partial \bar{u}_i}{\partial x_j} + \frac{\partial \bar{u}_j}{\partial x_i}\right) + T_{ij}\right\}, \tag{6}$$

where

$$T_{ij} = \bar{u}_i \bar{u}_j - \overline{u_i u_j} \tag{7}$$

is the subgridscale tensor. The filtered fields do not need to be resolved at scales smaller than Δx, since they do not contain fluctuations under this scale. Therefore, they can be properly represented by the computer, provided proper numerical schemes are used. The main problem lies in the subgrid-scale tensor: when expressed in terms of fluctuations with respect to the filtered field, certain terms remain unknown. The equations of motion for the filtered field have analogies with the Reynolds equations for the mean flow in non-homogeneous turbulence, but terms other than $-\overline{u_i' u_j'}$ arise in the LES.

In the LES, we have to solve the Navier-Stokes equations for the filtered field (large scales) modified by supplementary subgrid-scale terms which we do not know. Reviews of LES methods may be found in [1, 4].

The same analysis may be given for a scalar T (not necessarily passive) of molecular diffusivity κ convected by the flow. It satisfies

$$\frac{\partial T}{\partial t} + \frac{\partial}{\partial x_j}(T u_j) = \frac{\partial}{\partial x_j}\left\{ \kappa \frac{\partial T}{\partial x_j} \right\}. \tag{8}$$

If the low-pass filter $\bar{G}_{\Delta x}$ is applied to this equation, we find

$$\frac{\partial \bar{T}}{\partial t} + \frac{\partial}{\partial x_j}(\bar{T} \bar{u}_j) = \frac{\partial}{\partial x_j}\left\{ \kappa \frac{\partial \bar{T}}{\partial x_j} + \bar{T}\bar{u}_j - \overline{T u_j} \right\}. \tag{9}$$

Here, again, the question of modelling the subgrid scalar fluxes is posed.

The problem of the subgrid-scale modelling is a particular case of the passage from 'micro' to 'macro', where the laws governing a medium are known at a microscopic level, and evolution laws at a macroscopic level are sought. Here, in turbulence, the 'microscopic' level corresponds to the individual fluid particle obeying the Navier-Stokes equations; the 'macroscopic' level represents the filtered field.

From a mathematical point of view, the LES problem is not very well posed. Indeed, let us consider the time evolution of the fluid as the motion of a point in what resembles a phase space of very large dimension. At some initial instant, the flow computed with LES will differ from the actual flow, due to the uncertainty contained in the subgrid scales. This initial difference between the actual and the computed flow will grow, due to nonlinear effects, as in a dynamical system having a chaotic behaviour. Therefore, the two points will separate in phase space, and, as time goes on, the LES will depart from reality. However, as will be seen below, LES allows to predict the statistical characteristics of turbulence, as well as the dynamics of coherent vortices and structures.

2.2. Eddy-viscosity and diffusivity

In order to model the subgrid terms, we will now make an eddy-viscosity and eddy-diffusivity assumption. More specifically, we write

$$T_{ij} = 2\nu_t \, \bar{S}_{ij} + \tfrac{1}{3} T_{ll} \delta_{ij}, \tag{10}$$

where

$$\bar{S}_{ij} = \frac{1}{2}\left(\frac{\partial \bar{u}_i}{\partial x_j} + \frac{\partial \bar{u}_j}{\partial x_i}\right) \tag{11}$$

is the deformation tensor of the filtered field. The LES momentum equation becomes

$$\frac{\partial \bar{u}_i}{\partial t} + \bar{u}_j \frac{\partial \bar{u}_i}{\partial x_j} = -\frac{1}{\rho_0}\frac{\partial \bar{P}}{\partial x_i} + 2\frac{\partial}{\partial x_j}\left\{(\nu + \nu_t)\bar{S}_{ij}\right\}, \tag{12}$$

$\bar{P} = \bar{p} - (1/3)\rho_0 T_{ll}$ being a modified pressure, determined with the help of the filtered continuity equation (still valid on a regular mesh). For the scalar, we introduce an eddy diffusivity κ_t, as follows

$$\bar{T}\bar{u}_j - \overline{Tu_j} = \kappa_t \frac{\partial \bar{T}}{\partial x_j}, \tag{13}$$

to yield

$$\frac{\partial \bar{T}}{\partial t} + \bar{u}_j \frac{\partial \bar{T}}{\partial x_j} = \frac{\partial}{\partial x_j}\left\{(\kappa + \kappa_t)\frac{\partial \bar{T}}{\partial x_j}\right\}. \tag{14}$$

The eddy diffusivity is related to the eddy viscosity by the relation

$$P_r^{(t)} = \frac{\nu_t}{\kappa_t}, \tag{15}$$

where $P_r^{(t)}$ is a turbulent Prandtl number which will be specified below.

For compressible turbulence, we will assume that the subgrid scales are not far from incompressibility, and write compressible the Navier-Stokes equations for the filtered fields, with the above incompressible eddy-coefficients supplementing the molecular (viscous and diffusive) ones. This is certainly justified away from the shocks. In the shock region, and although the eddy viscosity is no longer physically justified, it may have a favourable effect by contributing to the stabilization of the shock.

The question is now to determine the eddy viscosity $\nu_t(\mathbf{x}, t)$. Notice that this eddy-viscosity assumption, in the framework of which we will be working here, is rather questionable. We expect, however, that the information about the physics of turbulence derived with this concept may help to improve it.

2.3. SMAGORINSKY'S MODEL

The most widely used eddy-viscosity model was proposed by Smagorinsky [2]. He was looking for an eddy-viscosity simulating in some way the three-dimensional Kolmogorov energy cascade in the subgrid scales. A local mixing-length assumption is made, in which the eddy viscosity is assumed to be proportional to the subgrid-scale characteristic length Δx, and to a characteristic turbulent velocity $v_{\Delta x} = \Delta x|\bar{S}|$. Here $|\bar{S}|$ is a typical velocity gradient at Δx, determined with the aid of the second invariant of the filtered-field deformation tensor $\bar{S}_{ij}$ defined in (11). Smagorinsky's eddy viscosity reads

$$\nu_t = (C_S \Delta x)^2 |\bar{S}|, \tag{16}$$

with $|\bar{S}| = \sqrt{2\bar{S}_{ij}\bar{S}_{ij}}$. If we assume that $k_C = \pi/\Delta x$, the cutoff wavenumber in Fourier space, lies within a $k^{-5/3}$ Kolmogorov cascade, we can adjust the constant C_S so that the ensemble-averaged subgrid kinetic-energy dissipation is identical to ε. We find

$$C_S \approx \frac{1}{\pi}\left(\frac{3C_K}{2}\right)^{-3/4}. \tag{17}$$

This yields $C_S \approx 0{\cdot}18$ for a Kolmogorov constant $C_K = 1{\cdot}4$. In fact, the dynamic-model ideas (see [5]) will consist in a local adjustment of C_S, basically to reduce the eddy-viscosity in places where turbulence is not totally developed, or during transition.

It should be noted that an existence theorem, uniqueness and regularity concerning the LES equations with Smagorinsky's model was derived by Lions [6].

We will discuss the performance of Smagorinsky's model in various applications which will be presented below. We will now present a different point of view of LES when working in Fourier space.

3. LES in spectral space

3.1. Spectral eddy viscosity and diffusivity

The formalism of spectral eddy viscosity is due to Kraichnan ([2], see also [3, 7, 8]) in the case of a Kolmogorov subgrid-scale spectrum. We adapt it here to a wider range of spectra, and to a scalar convected by the flow.

We assume that the Navier-Stokes formalism is written in Fourier space (which requires periodicity in the three spatial directions), and consider the cutoff wave number $k_C = \pi\Delta x^{-1}$ already envisaged above. We define a sharp low-pass filter by setting equal to zero the velocity and scalar amplitudes at wave vectors whose moduli are larger than k_C. Let us first consider the kinetic-energy and scalar transfers given by the EDQNM theory[1] ([1]). We assume first $k \ll k_C$ (both modes being larger than k_i, the kinetic-energy peak). Then we can write the spectral evolution equations for the supergrid-scale velocity, $\bar{E}(k,t)$, and scalar, $\bar{E}_T(k,t)$ spectra as

$$\left(\frac{\partial}{\partial t} + 2\nu k^2\right)\bar{E}(k,t) = T_{<k_C}(k,t) + T_{sg}(k,t), \tag{18}$$

$$\left(\frac{\partial}{\partial t} + 2\kappa k^2\right)\bar{E}_T(k,t) = T^T_{<k_C}(k,t) + T^T_{sg}(k,t), \tag{19}$$

with

$$T_{sg}(k,t) = -2\nu_t^\infty k^2 \bar{E}(k,t), \tag{20}$$

$$\nu_t^\infty = \frac{1}{15}\int_{k_C}^\infty \theta_{0pp}\left[5E(p,t) + p\frac{\partial E(p,t)}{\partial p}\right]\mathrm{d}p, \tag{21}$$

$$T^T_{sg}(k,t) = -2\kappa_t^\infty k^2 \bar{E}_T(k,t), \tag{22}$$

$$\kappa_t^\infty = \frac{2}{3}\int_{k_C}^\infty \theta^T_{0pp}E(p,t)\,\mathrm{d}p, \tag{23}$$

where θ_{kpq} and θ^T_{kpq} are nonlinear triple-correlation relaxation times of the EDQNM theory. The supergrid-scale transfers $T_{<k_C}(k,t)$ and $T^T_{<k_C}(k,t)$ correspond to triad interactions whose wave numbers lie in the supergrid range, and hence do not need any modelling, since they can be calculated exactly in the large-eddy simulation. Here, the nonlocal transfers from the supergrid to the subgrid scales have been evaluated with the aid of leading-order expansions with respect to the small parameter k/k_C.

Let us start by assuming a $k^{-5/3}$ inertial range at wave numbers greater than k_C. We obtain

$$\nu_t^\infty = 0{\cdot}441 {C_K}^{-3/2} \left[\frac{E(k_C)}{k_C}\right]^{1/2}, \tag{24}$$

$$\kappa_t^\infty = \frac{\nu_t^\infty}{P_r^{(t)}} \tag{25}$$

with

$$P_r^{(t)} = 0{\cdot}6. \tag{26}$$

The latter value is in fact the highest value permitted by the EDQNM theory (see [1], for a discussion of this point). If we assume, for instance, a Kolmogorov constant of 1·4 in the energy cascade, the constant in front of (24) will be 0·267. When k is close to k_C, the above concept of spectral eddy viscosity and eddy diffusivity can be generalized for a $k^{-5/3}$ inertial range extending over wave numbers larger than k_C. It is possible, with the aid of the EDQNM approximation, to calculate the subgrid-scale transfers, corresponding to triadic interactions where at least one of the wave numbers p and q is greater than k_C. This allows us to define two functions $\nu_t(k|k_C)$ and $\kappa_t(k|k_C)$, respectively, the eddy viscosity in spectral space ([3] and the eddy diffusivity in spectral space ([8]), such that

$$T_{sg}(k,t) = -2\nu_t(k|k_C)k^2\ \bar{E}(k,t), \tag{27}$$

$$T^T_{sg}(k,t) = -2\kappa_t(k|k_C)\ k^2\bar{E}(k,t). \tag{28}$$

The functions $\nu_t(k|k_C)$ and $\kappa_t(k|k_C)$ are such that

$$\nu_t(k|k_C) = K(k/k_C)\nu_t^\infty, \tag{29}$$

$$\kappa_t(k|k_C) = C(k/k_C)\kappa_t^\infty, \tag{30}$$

where ν_t^∞ and κ_t^∞ are the asymptotic values given by (24, 25 and 26). As shown by Kraichnan [3], $K(x)$ is approximately constant and equal to 1, except in the vicinity of $k/k_C = 1$ where it displays a strong overshoot (cusp-behaviour), due to the predominance of semi-local transfers across k_C. It was shown in [8] that $C(x)$ behaves qualitatively as $K(x)$ (plateau at 1 and positive cusp), and that the spectral turbulent Prandtl number $\nu_t(k|k_C)/\kappa_t(k|k_C)$ is approximately constant (and thus equal to 0·6).

In fact, the function $K(x)$ can be put in the form

$$K(x) = 1 + \nu_n^* x^{2n}, \tag{31}$$

with $2n \approx 3{\cdot}7$ ([7, 8]). We propose to determine ν_n^* by considering the energy balance between explicit and subgrid-scale transfers. This yields

$$\int_0^{k_C} 2\nu_t k^2 E(k,t)\,\mathrm{d}k = \varepsilon,$$

which, in an infinite Kolmogorov inertial range, leads to

$$1 + \frac{1}{1+(3n/2)}\nu_n^* = \frac{2}{3 \times 0{\cdot}441}. \tag{32}$$

We will return to this expression below, when we shall be working in physical space in terms of generalized hyperviscosities.

Let us mention that the use of the subgrid-scale transfers (27), (28) allows us to solve numerically the EDQNM kinetic energy and passive scalar evolution equations at zero molecular viscosity and conductivity in the self-similar decaying regime (for $k \leqslant k_C$), as shown by [7, 8].

3.2. LES OF ISOTROPIC TURBULENCE

Let us now return to the evolution equations (in spectral space) of the instantaneous filtered fields (for $|\mathbf{k}| < k_C$)

$$\left(\frac{\partial}{\partial t} + \nu k^2\right)\bar{\hat{u}}_i(\mathbf{k},t) = t_{<k_C}(\mathbf{k},t) + t_{sg}(\mathbf{k},t), \tag{33}$$

$$\left(\frac{\partial}{\partial t} + \kappa k^2\right)\bar{\hat{T}}(\mathbf{k},t) = t^T_{<k_C}(\mathbf{k},t) + t^T_{sg}(\mathbf{k},t), \tag{34}$$

with the usual distinction between the explicit supergrid transfers, still calculated by a truncation for $k, p, q \leqslant k_C$ of the nonlinear terms involved in Navier–Stokes equations in Fourier space (see [3]), and the unknown subgrid-scale transfers. We propose to model the latter with the aid of $\nu_t(k|k_C)$ and $\kappa_t(k|k_C)$ introduced in (27, 28), namely

$$t_{sg}(\mathbf{k},t) = -\nu_t(k|k_C)k^2\overline{\hat{u}}_i(\mathbf{k},t), \tag{35}$$

$$t^T_{sg}(\mathbf{k},t) = -\kappa_t(k|k_C)k^2\overline{\hat{T}}(\mathbf{k},t). \tag{36}$$

This subgridscale modelling is justified at the energetic transfer level, in the sense that, when we write the exact evolution equations for the spectra of $\overline{\hat{u}}$ and $\overline{\hat{T}}$ as they arise from (33, 34), we obtain the EDQNM subgridscale transfers calculated in (27, 28). The results of the spectral-cusp eddy viscosity applied to LES of decaying three-dimensional isotropic turbulence are satisfactory. The first calculations of this type at a very low resolution were done in [7, 8], respectively for the momentum equation and the passive scalar. Figures 1(a) and 1(b) show the decaying kinetic-energy and passive scalar spectra obtained in analogous LES at a resolution of 128^3 Fourier modes carried out by [9] (see also [10]). The initial velocity and scalar spectra are proportional, with a Gaussian ultraviolet behaviour and a k^8 infrared spectrum. It can be checked that Kolmogorov and Corrsin-Oboukhov $k^{-5/3}$ cascades result. Afterwards, the kinetic-energy spectrum decays self-similarly, with a slope between $-5/3$ and -2. The scalar

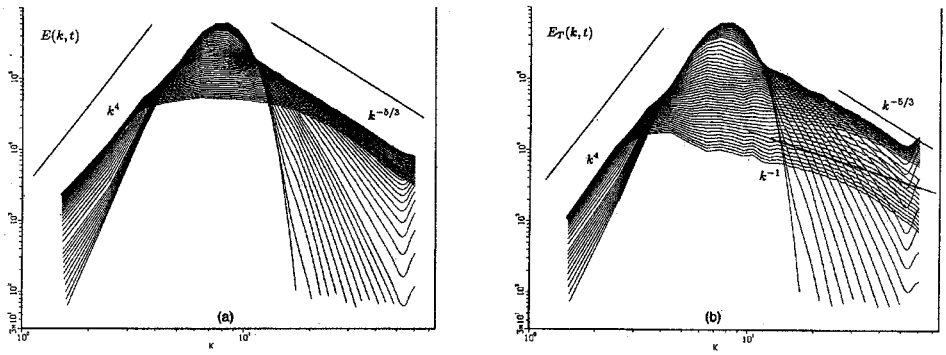

Figure 1. 3D isotropic decaying turbulence, resolution 128^3; decay of kinetic-energy (a) and passive-scalar (b) spectra, calculated from the LES of [9] with the spectral-cusp eddy viscosity.

spectrum seems to have a very short inertial-convective range close to the cutoff, and a very wide range shallower than k^{-1} in the large scales. This range was explained by [11] as due to the quasi two-dimensional character of the scalar diffusion in the large scales, leading to large-scale intermittency of the scalar.

3.3. THE SPECTRAL BACKSCATTER

Let us look now at the infrared ($k \to 0$) spectra obtained in Figures 1(a) and 1(b). The initial slope is k^8, as already stressed, and we see the formation of k^4 spectra. These spectra were predicted with the aid of two-point closures such as EDQNM[2] (see [12]) many years before they could be observed in the LES of [9, 10]. The derivation is the following: let k_i and k_i^T be, respectively, the peaks of the kinetic-energy and scalar spectra. The nonlocal interactions theory, where the nonlocal transfers are calculated to leading order in terms of expansions in powers of the small parameters k/k_i (resp. k/k_i^T) permits to show that nonlocal transfers are dominant in this infrared range, and, respectively, equal to

$$T(k,t) \approx \frac{14}{15} k^4 \int_{k_i}^{\infty} \theta_{0pp} \frac{E(p)^2}{p^2} \,\mathrm{d}p, \tag{37}$$

$$T^T(k,t) = \frac{4}{3} k^4 \int_{k_i^T}^{\infty} \theta_{0pp}^T \frac{E(p)}{p^2} E_T(p) \,\mathrm{d}p, \tag{38}$$

for the velocity and the scalar. These transfers, which arise in the rhs of the evolution equations for the spectra

$$\left(\frac{\partial}{\partial t} + 2\nu k^2\right) E(k,t) = T(k,t), \tag{39}$$

$$\left(\frac{\partial}{\partial t} + 2\kappa k^2\right) E_T(k,t) = T^T(k,t), \tag{40}$$

inject a k^4 spectrum in low wave numbers, through some kind of nonlinear resonant interaction between two modes $\approx k_i$. This spectral backscatter is responsible for the sudden appearance of k^4 infrared spectra when the initial spectra are sharply peaked, or simply $\propto k^s$ with $s > 4$.

This spectral backscatter phenomenon is important, since energy is thus injected at very low wave numbers, and, to our knowledge, two-point closure theories are the only ones which permit to predict it analytically[3]. Violent backscatter phenomena occur also in the statistical unpredictability theory both in two and three dimensions, as shown in [13].

Notice finally that, in the case of decaying isotropic three-dimensional turbulence, and for an initial infrared spectrum $\propto k^2$, an eddy-viscous term $\approx -2\nu_t(k|k_i)k^2E(k,t)$ is also present in $T(k,t)$, together with the k^4 backscatter. But both terms being of order $(k/k_i)^4$, they do not influence the evolution of the lhs of Equation (39), which is of the order $(k/k_i)^2$. This implies exact permanence of big eddies, with a k^2 infrared spectrum which is time invariant. The same holds for the scalar. If, on the other hand, turbulence is fed by some forcing concentrated around k_i, a stationary solution will imply an infrared balance between the backscatter and the eddy-viscous transfers, yielding a k^2 equipartition spectrum. A last remark is that the k^4 backscatter is negligible in LES where the cutoff k_C lies in the middle of a Kolmogorov range. Backscatter effects exist, which send back energy from the filtered to the subgrid scales. But, from an energetic point of view, they are contained in the cusp part of the plateau-cusp eddy viscosity considered above.

3.4. Spectral dynamic model

We will present below a local generalization of the plateau-cusp spectral eddy viscosity to physical space (structure-function model), which gives better results for isotropic turbulence as far as the Kolmogorov cascade is concerned. But let us show now an adaptation of the spectral-cusp model to kinetic-energy spectra $\propto k^{-m}$ for $k > k_C$, when the exponent m is not necessarily equal to $5/3$. The eddy viscosity given by (21) is now

$$\nu_t^\infty = \frac{1}{15a_1}\frac{5-m}{m+1}\sqrt{3-m}\left[\frac{E(k_C)}{k_C}\right]^{1/2}, \tag{41}$$

for $m \leqslant 3$. The constant $1/(15a_1)$ multiplying the rhs of (41) and coming from the EDQNM theory for the kinetic-energy spectrum, is equal to $0{\cdot}31{C_K}^{-3/2}$. This expression, derived in [11], was used by Lamballais ([14, 15]) for LES for a plane channel (see below). The associated eddy diffusivity is

$$\kappa_t^\infty = \frac{4}{3a_3}\,\frac{\sqrt{3-m}}{m+1}\,\left[\frac{E(k_C)}{k_C}\right]^{1/2}, \tag{42}$$

and the turbulent Prandtl number

$$P_r^{(t)} = \frac{5-m}{20}\,\frac{a_3}{a_1}, \tag{43}$$

where the constant a_3 arises in the EDQNM scalar-spectrum equation. It is such that we recover $P_r^{(t)} = 0.6$ for $m = 5/3$, so that we find finally

$$P_r^{(t)} = 0{\cdot}18(5-m). \tag{44}$$

For $m > 3$, this scaling is no longer valid, and the eddy-viscosity and diffusivity coefficients will be set equal to zero. In the spectral dynamic model, the exponent m is determined through

the LES with the aid of a least-squares fit of the kinetic-energy spectrum close to the cutoff. The asymptotic eddy viscosity (41) is multiplied by the plateau-cusp function $K(k/k_C)$ defined above.

4. Return to physical space

4.1. STRUCTURE-FUNCTION MODEL

Now, let us consider the EDQNM eddy viscosity (still scaling on $\sqrt{E(k_C)/k_C}$) without cusp, and adjust the constant as proposed by [16], by balancing in the inertial range the subgridscale flux with the kinetic energy flux ε in the energy spectrum evolution equation[4]. This yields

$$\nu_t(k_C) = \tfrac{2}{3} C_K^{-3/2} \left[\frac{E(k_C)}{k_C} \right]^{1/2}. \tag{45}$$

The difficulty with such an eddy-viscosity (if the energy spectrum may be computed) is that it is uniform in space when used in physical space. Obviously, the eddy viscosity should take into account the intermittency of turbulence: there is no need for any subgrid-scale modelling in regions of space where the flow is laminar or transitional. On the other hand, it is essential to dissipate in the subgrid scales the local bursts of turbulence if they become too intense. Considering also that turbulence in the small scales may not be too far from isotropy, the authors of [11] proposed to return to the classical formulation (10) in the physical space, where the eddy viscosity is determined with the aid of (45). $E(k_C, \mathbf{x})$ is now a local kinetic energy spectrum, calculated in terms of the local second-order velocity structure function of the filtered field

$$F_2(\mathbf{x}, \Delta x) = \left\langle \|\overline{\mathbf{u}}(\mathbf{x}, t) - \overline{\mathbf{u}}(\mathbf{x} + \mathbf{r}, t)\|^2 \right\rangle_{\|\mathbf{r}\| = \Delta x} \tag{46}$$

as if the turbulence is three-dimensionally isotropic, with Batchelor's formula

$$F_2(\mathbf{x}, \Delta x) = 4 \int_0^{k_C} E(k) \left(1 - \frac{\sin(k\Delta x)}{k\Delta x} \right) \mathrm{d}k. \tag{47}$$

For a Kolmogorov spectrum this yields

$$\nu_t^{SF}(\mathbf{x}, \Delta x) = 0{\cdot}105 C_K^{-3/2}\, \Delta x\, [F_2(\mathbf{x}, \Delta x)]^{1/2}. \tag{48}$$

F_2 is calculated with a local statistical average of square velocity differences between **x** and the six closest points surrounding **x** on the computational grid. In some cases, the average may be taken over four points parallel in a given plane; in a channel, for instance, the plane is parallel to the boundaries. Notice also that, if the computational grid is not regular, interpolations of (48) have been proposed in [4], where they used the fact that the second-order velocity-structure function scales like $(\varepsilon r)^{2/3}$ in a Kolmogorov inertial range.

The structure-function model (SF) works well for decaying isotropic turbulence, where it yields a fairly good Kolmogorov spectrum ([11]), better than Smagorinsky's model (with $C_S = 0{\cdot}2$) and Kraichnan's spectral-cusp model.

The SF model gives also good results for free-shear flows, where it is able to stretch secondary thin longitudinal hairpin vortices between primary vortices (see [4]). However,

selective or filtered versions of it work better in this case (see below). The SF model permits also to go beyond transition in a temporal[5] compressible boundary layer upon an adiabatic wall at Mach 4·5 ([17]). But it does not work for transition in a boundary layer at low Mach (or incompressible) where, like Smagorinsky, it is too dissipative and prevents TS waves to degenerate into turbulence. This is still true within the four-point formulation in planes parallel to the wall, which eliminates the effect of the mean shear at the wall on the eddy viscosity. In fact, the spectrum $E_{\mathbf{x}}(k_C)$ determined by the isotropic formula (45) is too sensitive to the inhomogeneous low-frequency oscillations caused by the TS waves.

4.2. Selective and filtered SF models

To overcome the difficulty of dissipating too much the large quasi two-dimensional vortices or transitional waves, two improved versions of the SF model have been developed: the selective structure-function model (SSF), and the filtered structure-function model (FSF). The dynamic model in physical space (see [5]) is another way of adapting the eddy viscosity to the local conditions of the flow.

The SSF model was developed in [18]. The idea is to switch off the eddy viscosity when the flow is not three-dimensional enough. The three-dimensionalization criterion is the following: we measure the angle between the vorticity at a given grid point and the average vorticity at the six closest neighbouring points (or the four closest points in the four-point formulation). If this angle exceeds 20°, the most probable value according to simulations of isotropic turbulence at a resolution of $32^3 \sim 64^3$, the eddy viscosity is turned on. Otherwise, only the molecular dissipation is active. The constant arising in (48) is changed, and determined with the aid of LES of freely-decaying isotropic turbulence: we require that the eddy viscosity averaged over the computational domain should be the same in a selective structure-function model and a SF model simulation. It is found that the constant in (48) has to be multiplied by 1·56.

The SSF model works very well for isotropic turbulence and free-shear flows, as well as for a compression ramp at Mach 2·5 (see [18]). We have used it also with success in LES of a flow above a backward-facing step. The SSF model depends, however, upon the most probable angle of the next neighbours average vorticity, chosen above equal to 20°. In fact, this angle is a function of the resolution of the simulation, since it should go to zero with Δx, and may be with the type of flow considered. Progress in this model should be made by adjustment of this angle to the local grid.

The FSF model was developed by Ducros ([19]) and applied to a boundary layer at Mach 0·5 ([20]). Here, the filtered field $\bar{u}_i$ is submitted to a high-pass filter in order to remove low-frequency oscillations which affect $E_{\mathbf{x}}(k_C)$ in (45). The high-pass filter is a Laplacian discretized by second-order centered finite differences and iterated three times. It was shown in [19] that, for some 3D random or turbulent isotropic test fields, the eddy-viscosity (48) can be written as

$$\nu_t^{FSF}(\mathbf{x}, \Delta x) = 0{\cdot}0014\, C_K^{-3/2} \Delta x [\tilde{F}_2(\mathbf{x}, \Delta x)]^{1/2}, \tag{49}$$

where $\tilde{F}_2$ is the second-order velocity structure function of the high-pass filtered field. This model gives good results for transition in a spatially-developing boundary layer. This simulation (see [20]) was done for a weakly-compressible case at $M_\infty = 0{\cdot}5$, for an adiabatic plate. It is seen how a TS wave, to which a three-dimensional white noise perturbation is superposed upstream, propagates downstream. First, quasi two-dimensional billows of relatively low pressure and high vorticity form, then undergo some sort of staggered unstability, as predicted by

[21], while weak longitudinal high- and low-speed streaks develop at the wall. Finally, the staggered pattern breaks down into turbulence, within which the classical high- and low-speed streaks are observed, with ejection of hairpins above the latter. The FSF model is, however, not 'perfect' for the prediction of average quantities. It overestimates, in particular, the mean velocity in the logarithmic profile by about 15%. The same happens when it is applied to the incompressible channel ([14]). In the latter case, the spectral dynamic model presented above works better, as will be seen below.

4.3. Generalized hyperviscosities

One of the common drawbacks of the different versions of the SF model is the absence of cusp near k_C. We return to (32), where we take $n = 2$, which yields $2n = 4$, not far from the EDQNM 3·7 value. Then (32) yields $\nu_2^* = 2{\cdot}044$, so that an equivalent of the spectral-cusp eddy viscosity in physical space is for the subgrid-scale dissipative operator in the filtered Navier-Stokes equation

$$2\frac{\partial}{\partial x_j}[0{\cdot}661\,\nu_t^{SF}\bar{S}_{ij}] + 1{\cdot}351\left(\frac{\Delta x}{\pi}\right)^4 \nu_t^{SF}(\nabla^2)^3\bar{u}_i, \tag{50}$$

where ν_t^{SF} is given by (48). This model[6] was used by the authors of [22] in a LES of a rotating stratified jet subjected to baroclinic instability. They could show developments of primary and secondary instabilities of the thermal fronts very similar to what is observed in the atmosphere.

Notice that, as for Smagorinsky's, existence and uniqueness have been demonstrated by Lions [6] for a subgrid-scale dissipation of the type (50), where ν_t is replaced by ν, provided the exponent arising in the Laplacian is $\geqslant 2$.

If we want to have now in physical space a model equivalent to the spectral-dynamic model, the dissipative operator (50) has to be multiplied by the constant

$$\tilde{A} = \frac{\sqrt{12}}{5}\frac{5-m}{m+1}\sqrt{3-m}, \tag{51}$$

where m is the slope of the kinetic-energy spectrum at the cutoff, which has to be obtained dynamically in some way. This might be possible if at least one periodicity direction exists in the flow. For a scalar, the corresponding turbulent Prandtl number is given by (44).

Such a spectral-dynamic generalized hyperviscosity model should be tested on various shear flows, such as those presented below.

5. Mixing layer

We show now three-dimensional results of the filtered structure function model applied to a plane mixing layer in the temporal and spatial cases, respectively.

5.1. Temporal mixing layer

We consider in a fluid of constant density a mixing layer periodic in the streamwise and spanwise directions, initiated by a hyperbolic-tangent velocity profile, to which is superposed a small random perturbation. We take free-slip boundary conditions on the upper and lower boundary, and use pseudo-spectral conditions in the three dimensions of space. A LES

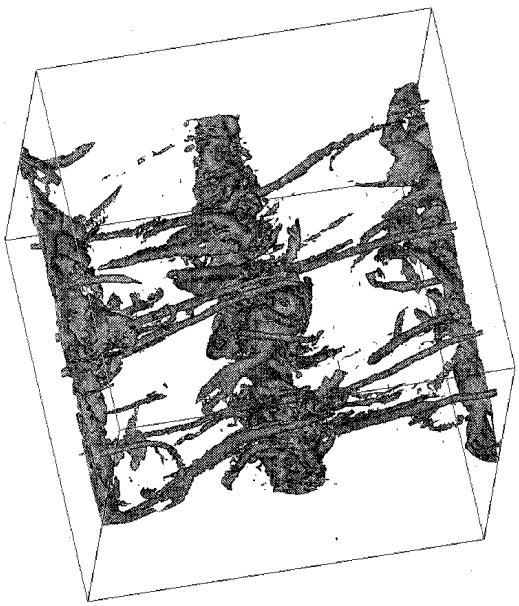

Figure 2. Vorticity field obtained in the LES of a temporal mixing layer forced quasi two-dimensionally.

incorporating the spectral-dynamic model shows the following results. If the perturbation is quasi two-dimensional, the mixing layer evolves into a set of big quasi two-dimensional vortices which both undergo pairing and stretch intense longitudinal hairpin vortices in the stagnation regions between them. Such a pattern is shown in Figure 2, taken from [23], and presenting a map of the vorticity modulus. This stretching of longitudinal vortices, which has been observed experimentally for a long time (see *e.g.* [24] and [25]), may be explained as follows: let us consider the vorticity equation, written for a perfect fluid of uniform density as

$$\frac{\mathrm{D}\boldsymbol{\omega}}{\mathrm{D}t} = \nabla \mathbf{u} : \boldsymbol{\omega} = \overline{\overline{S}} : \boldsymbol{\omega} + \tfrac{1}{2}\boldsymbol{\omega} \times \boldsymbol{\omega} = \overline{\overline{S}} : \boldsymbol{\omega}, \tag{52}$$

where $\mathrm{D}/\mathrm{D}t$ is the substantial derivative following the flow motion, and $\overline{\overline{S}}$ the deformation tensor, introduced in (11) for the filtered field. If we assume that the vorticity in the stagnation region between the vortices is weak, we may assume (at least initially) that the deformation tensor will not vary while the vorticity is stretched. Since the deformation tensor is real and symmetric, it admits eigenvectors (principal axes of deformation) which are orthogonal and can form a basis. Let s_1, s_2, s_3 be the three eigenvalues. Due to incompressibility, their sum is zero, so that one of these is positive (called here s_1) and another one at least is negative. Let s_2 be the smallest eigenvalue that is always negative. Working in the orthonormal frame formed by the eigenvectors $\mathbf{l}, \mathbf{t}, \mathbf{s}$ associated, respectively, with s_1, s_2, s_3, we observe that the vorticity components $\omega_1, \omega_2, \omega_3$ satisfy the following equations

$$\frac{\mathrm{D}\omega_1}{\mathrm{D}t} = s_1\omega_1, \qquad \frac{\mathrm{D}\omega_2}{\mathrm{D}t} = s_2\omega_2, \qquad \frac{\mathrm{D}\omega_3}{\mathrm{D}t} = s_3\omega_3, \tag{53}$$

and the vorticity will be stretched in the direction of the first principal axis, and compressed in the direction of the second. Generally, $\overline{\overline{S}}$ is not far from a pure deformation in the stagnation

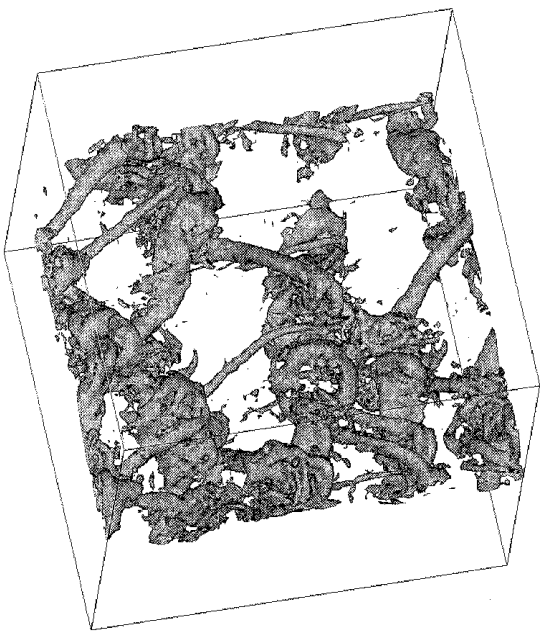

Figure 3. Vorticity field obtained in the LES of a temporal mixing layer undergoing helical pairing.

region, so that, approximately, **l** will be inclined 45° with respect to the mean flow, **s** will be spanwise, $s_3 = 0$ and $s_2 = -s_1$. Such a derivation unifies explanations given in [26] and [27]. Intense longitudinal hairpins were also found in [28] in temporal mixing-layer LES that used the spectral-cusp eddy viscosity. An interesting feature of these simulations is to show that longitudinal vorticity stretched between the primary Kelvin-Helmholtz vortices is rolled up within the cores of the big vortices, thus producing intense longitudinal vorticity fluctuations in the cores themselves. In Figure 2, the maximum longitudinal vorticity stretched is of the order of $4\omega_i$, which might be larger than the effective values reached experimentally. Actually, the efficiency of the longitudinal stretching could depend upon the amplitude of the initial perturbation and the Reynolds number.

Experiments in a developed mixing layer ([25]) show that the spanwise wavelength of the longitudinal vortices is of the order of two thirds of the longitudinal wavelength of the primary Kelvin-Helmholtz vortices between which they are stretched. This is precisely the most-amplified spanwise wavelength within a secondary-instability analysis of Stuart's vortices, as shown by Pierrehumbert and Widnall [29]. This instability, called the translative instability, corresponds, in fact, to a global in-phase oscillation of the big billows in the spanwise direction, and cannot explain the formation of the thin longitudinal hairpins. A plausible explanation could be that they do form according to the mechanisms corresponding to (53), but with a preferred spanwise wavelength imposed by the translative instability. Numerical simulations in the temporal or spatial cases need larger domains in the spanwise direction in order to validate the value of the preferred spanwise wavelength.

In fact, the numerical resolution of the three-dimensional Orr-Sommerfeld equation at large Reynolds number shows that the most-amplified mode in the 3D temporal mixing layer is indeed two-dimensional. By a naive application of this result, we might have believed that two-dimensional Kelvin-Helmholtz vortices would emerge from a weak three-dimensional random

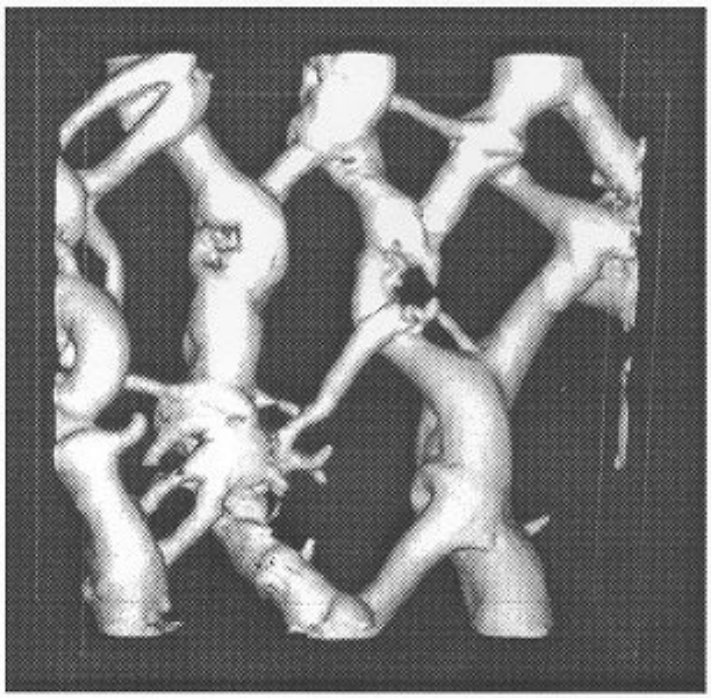

Figure 4. Low-pressure field obtained in a spectral-cusp LES in the helical-pairing case.

isotropic perturbation superposed upon the basic shear. But this is not at all what happens numerically. Instead, Comte *et al*. ([30, 31]), using DNS with pseudo-spectral methods at a resolution of 128^3 Fourier-wave vectors and a Reynolds number $U\delta_i/\nu = 100$, displayed the evidence for helical pairing, where vortex filaments oscillate out-of-phase in the spanwise direction, and reconnect, yielding a vortex-lattice structure. We have recovered the same dislocated pattern in LES (using the spectral-dynamic model) with the same forcing. Figure 3 shows the vorticity modulus obtained in such a simulation. Figure 4 shows the low-pressure field from an analogous LES using the spectral-cusp eddy viscosity. It confirms that low pressure is a very good indicator of big or intense vortices. Notice that at the end of the LES corresponding to Figure 3, the statistical data concerning velocity, rms velocity fluctuations and Reynolds stresses are in very good agreement with the experiments of unforced mixing layers. The simulation with a quasi two-dimensional forcing is less good from this standpoint.

The term 'helical pairing' was first proposed in [32], concerning highly three-dimensional pairings in a mixing-layer experiment. Afterwards, helical pairing was documented in the experiments of Browand and coworkers [33]. In the secondary-instability analysis of [29], the subharmonic instability found is identified with the previously observed helical pairing. Surprisingly, its amplification rate is lower than its translative-instability counterpart. Looking at DNS or LES of helical-pairing, it turns out that this is not exactly a 'secondary instability': we do not observe first the roll up of primary billows followed by a staggered deformation. Instead, oblique waves are seen to grow quickly, yielding directly the lattice structure of dislocated billows.

Finally, it may be interesting to see what can be said from the point of view of a scalar gradient when a scalar is transported passively by the flow. This may be very important if the

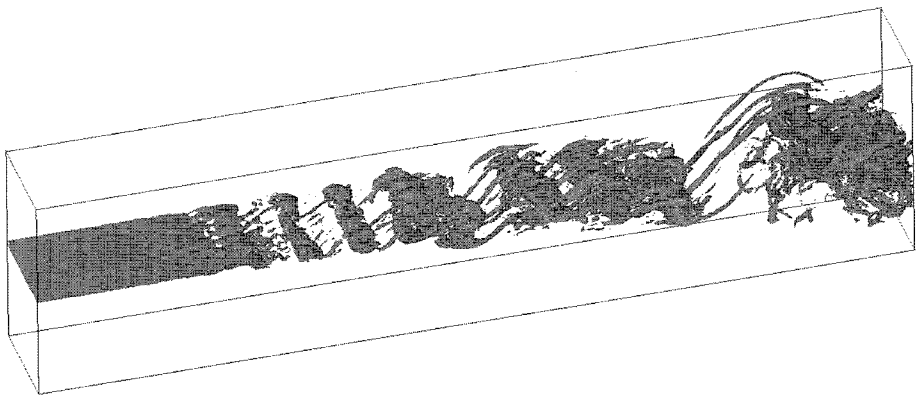

Figure 5. LES of an incompressible mixing layer forced upstream by a quasi two-dimensional random perturbation; the vorticity modulus is shown at a threshold $(2/3)\omega_i$.

two currents in the mixing layer react chemically, such as in combustion for instance. If the scalar σ satisfies $\mathrm{D}\sigma/\mathrm{D}t = 0$, its gradient follows the equation

$$\frac{\mathrm{D}}{\mathrm{D}t}\nabla\sigma = -\nabla\mathbf{u}|^t : \nabla\sigma. \tag{54}$$

If we are in a stagnation region between two vortices[7] and assume that the vorticity is small in front of the deformation, (54) may be approximated by

$$\frac{\mathrm{D}}{\mathrm{D}t}\nabla\sigma = -\overline{\overline{S}} : \nabla\sigma, \tag{55}$$

which yields for the three components of $\nabla\sigma$ in the principal axes of deformation

$$\frac{\mathrm{D}}{\mathrm{D}t}\frac{\partial\sigma}{\partial l} = -s_1\frac{\partial\sigma}{\partial l}, \qquad \frac{\mathrm{D}}{\mathrm{D}t}\frac{\partial\sigma}{\partial n} = -s_2\frac{\partial\sigma}{\partial n}, \qquad \frac{\mathrm{D}}{\mathrm{D}t}\frac{\partial\sigma}{\partial s} = -s_3\frac{\partial\sigma}{\partial s}. \tag{56}$$

This shows that the scalar gradient is compressed along the first principal axis of deformation, and stretched in the transverse direction, so that scalar gradients across the mixing-layer interface will steepen. In case of chemical reaction between the two layers, this will enhance the molecular exchanges at the interface, and favour the reaction.

5.2. Spatial mixing layers

The temporal approximation is only a crude approximation of a mixing layer spatially developing, where we work in a frame traveling with the average velocity between the two layers. We present now LES using the FSF model of a spatial mixing layer, initiated upstream by a hyperbolic-tangent velocity profile superposed on the average flow, plus a weak random forcing regenerated at each time step. The numerical code combines pseudo-spectral methods in the spanwise and transverse directions, and compact finite-difference schemes of sixth order in the streamwise direction (see [14]). This is a very precise code of accuracy comparable to a spectral method at an equivalent resolution. Free-slip conditions are still imposed upon the upper and lower boundaries. The outflow boundary condition is of the Orlanski's type [34].

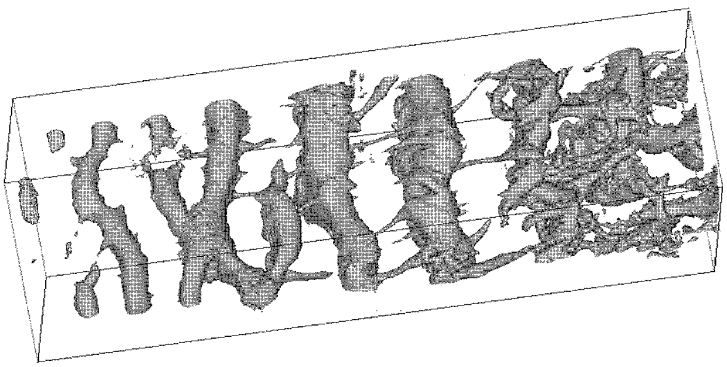

Figure 6. Same as Figure 5, but with a three-dimensional upstream white-noise forcing, low-pressure field.

With an upstream forcing consisting of a quasi two-dimensional random perturbation, intense longitudinal hairpins stretched between quasi 2D Kelvin-Helmholtz vortices are found again (Figure 5). An interesting feature found is that longitudinal vortices of the same sign may come close together and merge, thus contributing to the global self-similarity of the mixing layer. When the forcing is a three-dimensional random white noise, helical pairing occurs upstream, as indicated by the low-pressure maps of Figure 6. But none of these simulations has reached self-similarity, since the kinetic-energy spectra in the downstream region are steeper than $k^{-5/3}$, and rms velocity fluctuations have a departure of about 20% with respect to the experiments. Thus calculations in longer domains are necessary, in order to know in particular in the helical-pairing case whether quasi two-dimensionality might not be restored further downstream.

6. The channel flow

The results presented here were obtained by the numerical code just described above, with the spectral-dynamic eddy viscosity presented in Section 3. Here, the compact scheme is employed in the transverse direction, while pseudo-spectral methods are used in the longitudinal and spanwise directions, which are periodic. Calculations start with a parabolic Poiseuille velocity profile to which a small white-noise perturbation is superposed, and are run up to complete statistical stationarity, where a constant flow rate of average velocity U_m is assumed across the section. The channel has a width $2h$, and we define the macroscopic Reynolds number by $R_e = 2hU_m/\nu$. It does not change with time during the computation, since U_m is conserved. We will define also a microscopic Reynolds number $h^+ = v_* h/\nu$, based on the friction velocity in the turbulent regime. The kinetic-energy spectrum that allows us to determine the eddy-viscosity is calculated in each plane parallel to the walls[8].

We will present two LES at $R_e = 6666$ ($h^+ = 204$, case A) and $R_e = 14000$ ($h^+ = 389$, case B). They are, respectively, subcritical and supercritical with respect to the linear-stability analysis of the Poiseuille profile. In the two simulations there is a grid refinement close to the wall, in order to simulate accurately the viscous sublayer. Figure 7 shows for case A the exponent m arising in the energy spectrum at the cutoff, as a function of the distance to the wall y^+. Regions where $m > 3$ correspond to a zero eddy viscosity and hence a direct-numerical simulation. This is the case, in particular, close to the wall, up to $y^+ \approx 12$, where we know that longitudinal velocity fluctuations are very intense, due to the low- and

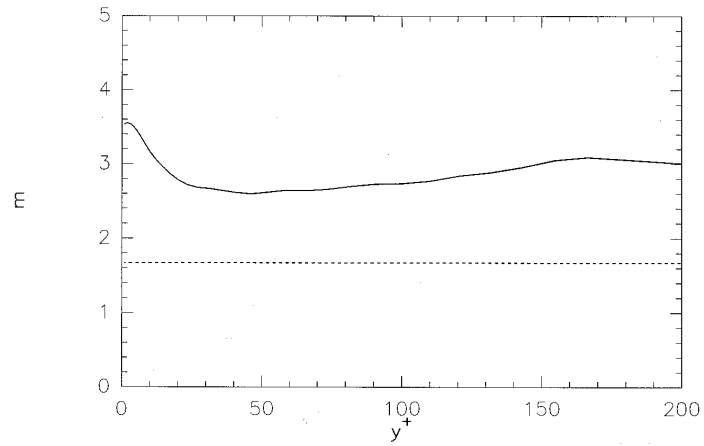

Figure 7. Spectral-dynamic LES of the channel flow (case A), exponent $m(y^+)$ of the kinetic-energy spectrum at the cutoff.

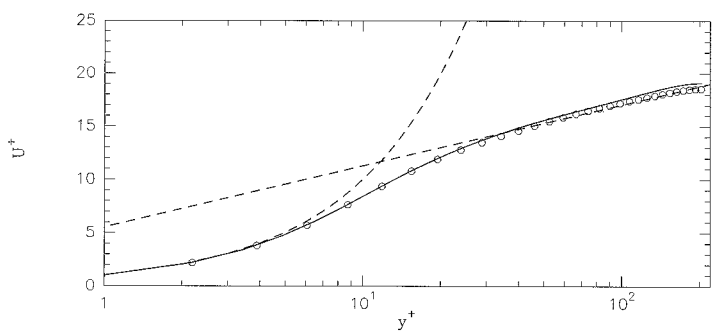

Figure 8. Same LES as Figure 7. Comparison of the mean velocity profile (solid line) versus Piomelli's [35] dynamic-model simulations (symbols).

high-speed streaks. Therefore, and since the first point is very close to the wall ($y^+ = 1$), our LES has the interesting property of becoming a DNS in the vicinity of the wall, which enables us to capture events which occur in this region. Figure 8 shows the mean velocity profile in case A, compared with the LES of Piomelli [35] using the dynamic model of [5]. The latter is

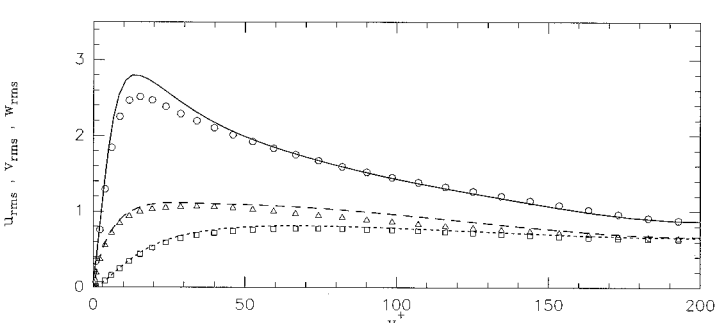

Figure 9. Same as Figure 8, but for the rms velocity fluctuations, from top to bottom longitudinal, spanwise and transverse.

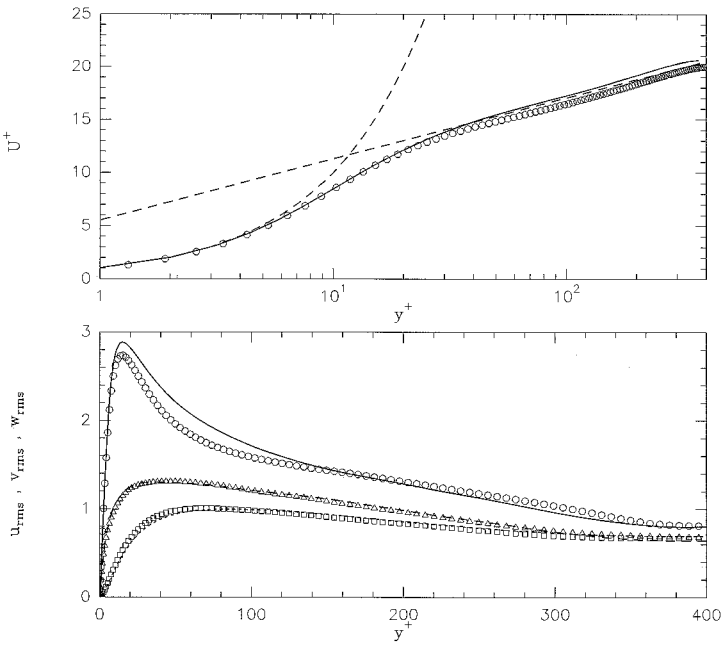

Figure 10. Turbulent channel flow, comparisons of the spectral-dynamic model (solid lines, $h^+ = 389$) with the DNS of Kim ([36], symbols, $h^+ = 395$); (a) mean velocity, (b) rms velocity components.

known to agree very well with experiments at these low Reynolds numbers. Our simulation coincides, with the right value for the Karman constant. On the other hand, a LES carried out with the classical spectral-cusp model with $m = 5/3$ gives an error of 20% for the Karman constant. Figure 9 shows, for case A, the rms velocity fluctuations compared with Piomelli. The agreement is still very good, with a correct prediction of the longitudinal velocity fluctuations peak, corresponding to a maximum intensity for the low- and high-speed streaks. Concerning the supercritical case, the LES of case B are in very good agreement with a DNS at $h^+ = 395$ carried out by [36], both for the mean velocity and the rms velocity components. The latter are shown on Figure 10. Notice that LES allows to reduce the computational cost by a factor of the order of 100, which is huge. We have checked that, in the LES of Figure 10 and very close to the wall, the spanwise vorticity fluctuations are much higher than their longitudinal and transverse counterparts. As shown in ([20]), this is due to excursions of high spanwise vorticity occurring under the high-speed streaks, which are responsible for most of the drag at the wall.

7. Conclusion

We have presented the general framework of large-eddy simulations (LES), where subgrid-scale motions are filtered out, their effect being represented by eddy-viscosity and eddy-diffusivity coefficients in the supergrid-scale motions. We have described Smagorinsky's model, which is the most-widely used for engineering applications. Later, we have presented a different point of view, where the filtering is a sharp low-pass filter in Fourier space. We have presented Kraichnan's spectral eddy viscosity, and generalized it to a spectral eddy diffusivity. We have demonstrated, using the nonlocal interaction theory applied to a stochastic model of

isotropic turbulence, how a k^4 backscatter arises in three dimensions, with a k^3 equivalent in two dimensions. We have confirmed the existence of such a spectral backscatter in large-eddy simulations. We have also presented the spectral-dynamic model, which is a generalization of the spectral eddy coefficients that allow to deal with laminar and transitional situations. Returning to physical space, we have reinterpreted these models in terms of velocity-structure functions and generalized hyperviscosity models.

We have applied the selective structure-function model to a temporal and spatially-growing mixing layer. Depending upon the quasi two-dimensional or three-dimensional character of the initial or upstream weak perturbation, we have shown how the flow could bifurcate from a quasi two-dimensional state (where longitudinal hairpins are stretched between the Kelvin-Helmholtz vortices) to a helical-pairing configuration of dislocated vortices. In the former case, consideration of the vorticity equation permits to show how the vorticity is stretched in the direction of the first principal axis of deformation. A convected scalar gradient, on the contrary, is reduced in this direction, and intensified across the interface. Returning to the hairpin stretching, we have found in the spatially-growing case that two longitudinal vortices may merge.

We have also applied these models to turbulent channel flow at a subcritical ($h^+ = 204$) and supercritical ($h^+ = 389$) wall Reynolds number. In the two cases, the results are in excellent agreement with experiments and direct-numerical simulations. Compared with the latter at same Reynolds number, the LES reduces the computational cost by a factor of the order of one hundred.

8. Acknowledgements

We are indebted to P. Begou for computational support. This work was sponsored by *Institut Universitaire de France*, CNRS, INPG and UJF.

Notes

[1] Kraichnan [2] considered the Test-Field Model (TFM) instead of the Eddy-Damped Quasi-Normal Markovian theory (EDQNM), but results are the same in a Kolmogorov inertial range.

[2] This is also valid for TFM, DIA (Direct-Interaction Approximation) and even Quasi-Normal theories.

[3] In two-dimensional turbulence, a k^3 backscatter also arises (see [1]).

[4] The same was done in order to obtain (32).

[5] Periodic in the flow direction.

[6] With an equivalent formulation for the density and a turbulent Prandtl number of 0·6.

[7] Situation where longitudinal hairpin vortices are likely to form.

[8] In fact, the original formula for the spectral-eddy viscosity considered to model a three-dimensional spectrum. It is possible, in the isotropic case and when spectra decrease as a power law, to relate the two-dimensional to the three-dimensional spectrum. A LES of the channel seems to be insensitive to the particular spectrum chosen.

References

1. M. Lesieur, *Turbulence in Fluids, (Third Edition)*, Dordrecht: Kluwer Academic Publishers (1997) 515pp.
2. J. Smagorinsky, General circulation experiments with the primitive equations. *Mon. Weath. Rev.* 91 (1963) 99–164.
3. R. H. Kraichnan, Eddy viscosity in two and three dimensions. *J. Atmos. Sci.* 33 (1976) 1521–1536.
4. M. Lesieur and O. Métais, New trends in large-eddy simulations of turbulence. *Ann. Rev. Fluid Mech.* 28 (1996) 45–82.
5. M. Germano, U. Piomelli, P. Moin and W. Cabot, A dynamic subgrid-scale eddy-viscosity model. *Phys. Fluids A.* 3 (1991) 1760–1765.
6. J. L. Lions, *Quelques Méthodes de Résolution des Problèmes aux Limites Non Linéaires*. Paris: Dunod (1969) 554pp.

7. J. P. Chollet and M. Lesieur, Parameterization of small scales of three-dimensional isotropic turbulence utilizing spectral closures. *J. Atmos. Sci.* 38 (1981) 2747–2757.
8. J.P. Chollet and M. Lesieur, Modélisation sous maille des flux de quantité de mouvement et de chaleur en turbulence tridimensionnelle isotrope. *La Météorologie* 29–30 (1982) 183–191.
9. M. Lesieur and R. Rogallo, Large-eddy simulation of passive-scalar diffusion in isotropic turbulence. *Phys. Fluids A* 1 (1989) 718–722.
10. M. Lesieur, O. Métais and R. Rogallo, Etude de la diffusion turbulente par simulation des grandes échelles. *C.R. Acad. Sci. Paris* Ser II 308 (1989) 1395–1400.
11. O. Métais and M. Lesieur, Spectral large-eddy simulations of isotropic and stably-stratified turbulence. *J. Fluid Mech.* 239 (1992) 157–194.
12. M. Lesieur and D. Schertzer, Amortissement auto similaire d'une turbulence à grand nombre de Reynolds. *J. de Mécanique* 17 (1978) 609–646.
13. O. Métais and M. Lesieur, Statistical predictability of decaying turbulence. *J. Atmos. Sci*. 43 (1986) 857–870.
14. E. Lamballais, *Simulations Numériques de la Turbulence dans un Canal Plan Tournant*. Thèse de l'Institut National Polytechnique de Grenoble (1995) 178pp.
15. E. Lamballais, M. Lesieur, and O. Métais, Influence d'une rotation d'entraînement sur les tourbillons cohérents dans un canal. *C. R. Acad. Sci. Paris* Ser II 323 (1996) 95–101.
16. D. C. Leslie and G. L. Quarini, The application of turbulence theory to the formulation of subgrid modelling procedures. *J. Fluid Mech.* 91 (1979) 65–91.
17. F. Ducros, P. Comte and M. Lesieur, Direct and large-eddy simulations of a supersonic boundary layer. In: N. Kasagi and K. Suzuki (eds.), *Turbulent Shear Flows IX*, Berlin: Springer-Verlag, (1995) pp. 283–300.
18. E. David, *Modélisation des Écoulements Compressibles et Hypersoniques: Une Approche Instationnaire*. Thèse, Institut National Polytechnique de Grenoble (1993) 179pp.
19. F. Ducros, *Simulations Numériques Directes et des Grandes Echelles de Couches Limites Compressibles*. Thèse, Institut National Polytechnique de Grenoble (1995) 180pp.
20. F. Ducros, P. Comte and M. Lesieur, Large-eddy simulation of transition to turbulence in a boundary-layer developing spatially over a flat plate. *J. Fluid Mech.* 326 (1996) 1–36.
21. T. Herbert, , Secondary instability of boundary layers. *Ann. Rev. Fluid Mech.* 20 (1988) 487–526.
22. E. Garnier, O. Métais and M. Lesieur, Instabilités primaires et secondaires dans un jet barocline. *C.R. Acad. Sci. Paris* Ser II b 323 (1996) 161–168.
23. J. Silvestrini, *Simulation des Grandes Échelles des Zones de Mélange: Application à la Propulsion Solide des Lanceurs Spatiaux*. Thèse de l'Institut National Polytechnique de Grenoble (1996) 150pp.
24. J. H. Konrad, *An Experimental Investigation of Mixing in Two-Dimensional Turbulent Shear Flows with Applications to Diffusion-Limited Chemical Reactions*. Ph.D. Thesis, California Institute of Technology (1976).
25. L. P. Bernal and A. Roshko, Streamwise vortex structure in plane mixing layer. *J. Fluid Mech.* 170 (1986) 499–525.
26. G. M. Corcos and S. J. Lin, The mixing layer: deterministic models of a turbulent flow. Part 2. The origin of the three-dimensional motion. *J. Fluid Mech.* 139 (1984) 67–95.
27. J. C. Neu, The dynamics of stretched vortices. *J. Fluid Mech.* 143 (1984) 253–276.
28. P. Comte and M. Lesieur, Coherent structures of mixing layers in large-eddy simulation. In: H. K. Moffatt (ed.) *Topological Fluid Dynamic*. Cambridge: Cambridge University Press (1989) pp. 649–658.
29. R. T. Pierrehumbert and S. E. Widnall, The two- and three-dimensional instabilities of a spatially periodic shear layer. *J. Fluid Mech.* 114 (1982) 59–82.
30. P. Comte, Y. Fouillet, M. A. Gonze, M. Lesieur, O. Métais, and X. Normand, Large-eddy simulations of free-shear layers. In: O. Métais and M. Lesieur (eds.) *Turbulence and coherent structures*. Kluwer Academic Publishers (1991) pp. 45–73.
31. P. Comte, M. Lesieur, and E. Lamballais, Large and small-scale stirring of vorticity and a passive scalar in a 3D temporal mixing layer. *Phys. Fluids A* 4 (1992) 2761–2778.
32. C. Chandrsuda, R. D. Mehta, A. D. Weir and P. Bradshaw, Effect of free-stream turbulence on large structure in turbulent mixing layers. *J. Fluid Mech.* 85 (1978) 693–704.
33. F. K. Browand and T. R. Troutt, A note on spanwise structure in the two-dimensional mixing layer. *J. Fluid Mech.* 93 (1980) 325–336.
34. I. Orlanski, A simple boundary condition for unbounded hyperbolic flows, *J. Comp. Phys.* 21 (1976) 251–269.
35. U. Piomelli, High Reynolds number calculations using the dynamic subgrid-scale stress model. *Phys. Fluids A* 5 (1993) 1484–1490.
36. R. A. Antonia, M. Teitel, J. Kim, and L. W. B. Browne, Low-Reynolds-number effects in a fully developed turbulent channel flow. *J. Fluid Mech.* 236 (1992) 579–605.